

Interfacial segregation of interacting vacancies and their role on the wetting critical properties of the Blume-Emery-Griffiths model

L. M. Luque , S. A. Grigera , and E. V. Albano*Instituto de Física de Líquidos y Sistemas Biológicos, UNLP-CONICET, La Plata 1900, Argentina*

(Received 11 January 2021; accepted 28 April 2021; published 12 May 2021)

We study the wetting critical behavior of the three-state ($s = \pm 1, 0$) Blume-Emery-Griffiths model using numerical simulations. This model provides a suitable scenario for the study of the role of vacancies on the wetting behavior of a thin magnetic film. To this aim we study a system confined between parallel walls with competitive short-range surface magnetic fields ($h_L = -|h_1|$). We locate relevant critical curves for different values of the biquadratic interaction and use a thermodynamic integration method to calculate the surface tension as well as the interfacial excess energy and determine the wetting transition. Furthermore, we also calculate the local position of the interface along the film and its fluctuations (capillary waves), which are a measure of the interface width. To characterize the role played by vacancies on the interfacial behavior we evaluate the excess density of vacancies, i.e., the density difference between a system with and without interface. We also show that the temperature dependence of both the local position of the interface and its width can be rationalized in term of a finite-size scaling description, and we propose and successfully test the same scaling behavior for the average position of the center of mass of the vacancies and its fluctuations. This shows that the excess of vacancies can be associated to the presence of the interface that causes the observed segregation. This segregation phenomena is also evidenced by explicitly evaluating the interfacial free energy.

DOI: [10.1103/PhysRevE.103.052803](https://doi.org/10.1103/PhysRevE.103.052803)

I. INTRODUCTION

The study and characterization of surfaces and interfaces is a topic relevant to many fields within physics, chemistry, material science, and others [1,2]. Considerable experimental and theoretical attention has been addressed to understanding common features of surfaces and interfaces at equilibrium [3–8] and far from it [9,10]. This broad interest is motivated not only by its numerous technological applications but also by the existence of many challenges at the basic level. Within this broad context, the influence of the presence of an additional phase at the interface between two phases has also been a source of experimental and theoretical studies. In particular, the phenomenon of enhancement of the density of the additional phase at the interface, known as “interfacial adsorption.” An experimental realization of this physical situation is provided by a two-component fluid system in equilibrium with its vapor phase [11]. From the point of view of statistical physics, which is the approach that will be followed in this paper, interfacial adsorption can be studied by means of three-state models, such as the Potts model or the Blume-Capel (BC) model. A straightforward way to observe interfacial adsorption is by confining the sample between two walls where competitive surface magnetic fields act. In this way, an interface between domains of different signs of the magnetization runs parallel to the confining walls, and vacancies adsorb preferentially along such an interface leading to interfacial adsorption, as reported by Selke [12]. It is also known that, depending on the temperature and the magnitude of the competitive surface fields, the interface between

domains undergoes localization-delocalization “transitions.” Those “effective” transitions are the precursors of the wetting transitions observed when the thermodynamic limit is properly taken. Interfacial adsorption has been observed by studying the localization-delocalization transition of the interface between domains of different magnetization in the BC model [13]. Furthermore, Fytas and Selke [14] have reported an extensive numerical study of wetting and interfacial adsorption in the BC model. To study wetting behavior in $d = 2$ dimensions, Fytas and Selke assumed that spins are fixed at the boundaries with two different states, “+1” and “−1,” with the addition of reduced couplings at one boundary. The adsorption of third state (“0” spins) at the interface between “−1” and “+1” rich regions is mainly characterized by measuring the interfacial adsorption W_0 , which accounts for the surplus of “0” spins caused by the presence of the interface. It is reported that due to the strong meandering of the interface, W_0 grows rapidly when approaching the wetting temperature. The existence of a singularity in the temperature derivative of W_0 at the wetting transition is conjectured. It is worth mentioning that the results of Fytas and Selke for the wetting transition of the BC model confined between walls are in agreement with previous results [13] and are found to obey the anisotropic scaling behavior for wetting transitions with short-range surface fields [13,15].

In a related context, great interest has also been attracted by the study of interfacial pinning induced by impurities. In fact, experimental and theoretical evidence [16,17] has confirmed that a magnetic interface can be pinned by uniformly distributed nonmagnetic impurities. The influence of

nonmagnetic fixed impurities placed at the center of an Ising ferromagnet confined between walls has been studied [18]. It is found that for a low density of impurities the wetting transition remains continuous (second order), while abrupt first-order transitions are observed when such a density increases [19]. In view of the reported change in the nature of the wetting transition caused by the presence of impurities in the case of the Ising ferromagnet, it is surprising that interfacial adsorption in the BC model does not affect the second-order nature of the wetting transition [13,14].

Within this broad context, the aim of the present paper is to contribute to understanding the role played by nonmagnetic impurities or vacancies in the wetting transition that occurs when ferromagnet confined between walls where competitive surface magnetic fields act. We will focus our attention on the Blume-Emery-Griffiths (BEG) model [20]. This model is based on the BC model [21,22], like its predecessor it contains an Ising-like term for interaction between spins, a term that controls the abundance of vacancies, and it incorporates an interaction term between the latter. In the present work we study the confined BEG model by means of extensive Monte Carlo simulations which are rationalized in terms of a recently proposed [13] anisotropic scaling approach. However, we take advantage of the biquadratic interaction term, which, depending on its sign favours either the formation of vacancy interfaces or clustering of vacancies and occupied sites. Our hypothesis is that if the vacancies tend to cluster, the interface behavior would be analogous to the one of the interfacial pinning induced by impurities [19] and the character of the transition would change. By using the approach discussed above, we are able to elucidate the role played by the nonmagnetic impurities in the character of the wetting transitions in the $d = 2$ dimensional BEG model. Furthermore, we use the thermodynamic integration technique to look for first-order wetting transitions. We show a simplified way to carry out this study by using a Wang-Landau algorithm, which allows us to directly calculate the free energy of the system.

Finally, we would like to mention that mobile vacancies could be relevant for the study of wetting upon adsorption on layered materials, e.g., when two bulky layers (of a single or different compound) are separated by a very thin layer of an additional species, as used in many micro and nanodevices. In fact, the influence of a transverse magnetic field on both layering and bulk-melting transitions in the BEG model has been studied by using a mean-field approach [23]. In this case, infinitely long slabs of a finite width with open boundary conditions were used for technical reasons, and competitive surface magnetic fields (as used in the present study) were not considered, except for the trivial case $h_1 = 0$. Also, it is worth to mention that layering transitions can be observed for $d > 2$, in contrast to the wetting transitions studied in this paper. Experimental evidence of layering transitions can be found in Refs. [24,25]. Another realization would be a binary surfactant mixture at the air-water interface undergoing phase separation: A defect line with mobile particles then could be created by colloidal particles bound also to the interface but trapped in a cylindrical potential well at the interface, created by suitable laser fields. This system would be a direct (qualitative) realization of the situation envisaged in our simple model.

The manuscript is organized as follows: in Sec. II we describe the main features of the BEG Hamiltonian together with a brief discussion of the simulation method. Section III is devoted to the presentation and discussion of our results within the framework of the finite-size scaling approach for wetting transitions with short-range surface fields [15], interfacial adsorption, dynamic on the wetting layers based on the vacancy excess profiles, and the thermodynamic integration method for the location of first-order wetting transitions. Finally, our conclusions are presented in Sec. IV.

II. MODEL AND METHODS

The study of a wetting transition, where the boundary induces the formation of a macroscopically thick film of the phase it favors, coexisting with the other phase separated by an interface at macroscopic distance from the boundary, requires us to consider the limit $L \rightarrow \infty$, where L is the thickness of the film. For any finite L in the antisymmetric thin film geometry, or thin strip geometry when one considers $d = 2$ dimensions rather than $d = 3$, one does not find a wetting transition but rather the “interface localization-delocalization transition” [26–35]: for temperature $T_c(L, h_1)$ but below the transition temperature T_b of the bulk, the interface between the coexisting phases is “delocalized,” freely fluctuating in the center of the film (or strip, respectively). Here by “center” we mean the plane (or line) $(L + 1)/2$, if we label the layers (rows) of the lattice parallel to the boundaries from $n = 1$ to $n = L$. However, for $T < T_c(L, h_1)$, the interface is tightly bound, and hence “localized,” near one of the boundaries. One predicts, however, that for large L , the transition temperature converges rapidly to the wetting temperature $T_w(h_1)$ of the semi-infinite system [29,30], and this prediction is consistent with numerical simulations [27,28,31–33,35]. Since simulations require systems with finite linear dimensions, we consider the Hamiltonian of the BEG model in a square lattice of geometry $L \times M$, where the dimensions L and M are perpendicular and parallel to the surface, respectively. This lattice has periodic boundary conditions along the x direction (where the lattice has length M) and free boundary conditions (walls) in the y direction, on which surface fields h_1 and h_L act. Capillary condensation like effects are then avoided, and phase coexistence still occurs [31]. However, when linear dimensions L, M are varied, ratios $L/\xi_\perp, M/\xi_\parallel$, with ξ_\perp and ξ_\parallel the correlation lengths, need to change in the same way (cf. Fig. 1) A schematic representation can be seen in Fig. 1.

The BEG Hamiltonian under these conditions has the following form:

$$\mathcal{H} = -J \sum_{\langle i, j \rangle} s_i s_j + D \sum_{i=1}^N s_i^2 - \alpha J \sum_{\langle i, j \rangle} s_i^2 s_j^2 - h_1 \sum_{i=1} s_i - h_L \sum_{i \in L} s_i, \quad (1)$$

where the spin variable s_i can take the values 1, 0 and -1 , $\langle i, j \rangle$ indicates sum over nearest neighbors and N is the total number of sites. J is the coupling constant which we take equals to 1 throughout the entire study, D is the crystal field, which favors the presence of vacancies when it is positive and

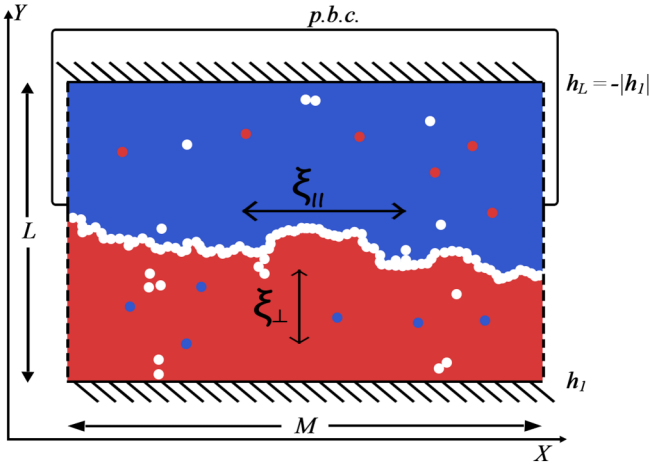


FIG. 1. Schematic description of the system geometry and its state at the wetting transition temperature $T_w(h_1)$. In that state, the interface has detached from the wall and is fluctuating in the middle of the lattice. It separates two domains with opposite magnetization, where the positive domain is represented with red and the negative one with blue. Vacancies are represented with white, and most of them are located there due to the interfacial adsorption. The choice of the linear lengths L and M , and the boundary conditions are indicated: periodic in the x direction and free in the y direction. The surface fields h_1 and $h_L = -|h_1|$ act on the latter. The correlation lengths are also shown: parallel ξ_{\parallel} and perpendicular ξ_{\perp} to the interface. These satisfy $\xi_{\parallel} \propto \xi_{\perp}^2$.

α is a parameter characterizing the biquadratic interaction that either favors nearest neighbors sites occupation when positive, or promotes the mixing of occupied sites with vacancies. The coupling constant J is homogeneous throughout the entire system, so the possibility of adding a different constant J_S for the edge spins is not considered as has been done in other studies [26,31–33,35–37]. The lattice parameter will be taken as a unit of length, so the total number of spins is equivalent to the product of the linear lengths of the system, $N = L \times M$. The surface fields, h_1 and h_L , act only on the spins of the first and last rows, respectively. These could be homogeneous or heterogeneous depending on the type of study performed. To study localization-delocalization pseudo transitions of the interface, that will correspond to true wetting critical transitions when the proper thermodynamical limit is taken, we considered competitive surface fields, $h_L = -|h_1|$ (see Fig. 1).

We have used two different methods for the numerical simulations: the usual Monte Carlo metropolis update [38] and the Wang-Landau algorithm for the evaluation of the density of states [39,40] in the implementation proposed by Belardinelli-Pereyra [41]. A detailed description of the simulation methods can be found in the Appendix.

III. RESULTS

A. Numerical simulations

The study and characterization of the localization-delocalization transitions and the interfacial adsorption, is performed by working in the ferromagnetic phase of the BEG phase diagram. Such a diagram, which was fully characterized in a previous work [42], consists of three different phases:

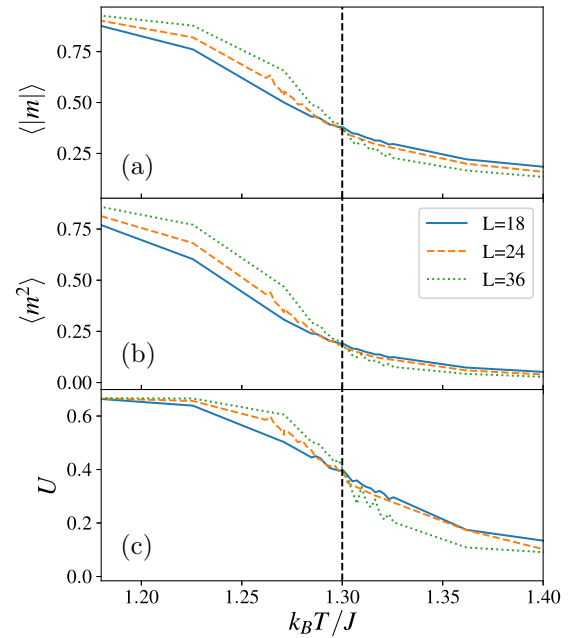


FIG. 2. Plots of the average absolute value of the magnetization $\langle |m| \rangle$ (a), the second moment of magnetization $\langle m^2 \rangle$ (b) and the fourth-order Binder cumulant U (c) as a function of the temperature $k_B T / J$, for $\alpha = 1$, $D = 3$ and $h_1 = 0.7$. Vertical lines indicate the location of the size-independent intersection point, which corresponds to the critical wetting temperature. In this case $k T_w(h_1) / J \simeq 1.30$.

ferromagnetic, paramagnetic, and quadrupolar, the later one with one sublattice filled with spins and the other with vacancies. The ferromagnetic-paramagnetic transition lines present first- and second-order transitions, separated by tricritical points. As it was mentioned before, localization-delocalization transitions that are observed in finite-confined samples, becomes true wetting transitions when the thermodynamic limit is properly taken [29,30]. Since for $\alpha = 0$ we recover the BC model that already exhibited wetting transitions [13,15], we take $\alpha > 0$, so it will favor the mixing of occupied sites with vacancies.

Based on the scaling theory for critical wetting [13,15], a particular value of the generalized aspect ratio (c) has been used:

$$\frac{L^{\nu_{\parallel}/\nu_{\perp}}}{M} = \frac{L^{2/1}}{M} = c = \frac{9}{8}, \quad (2)$$

where ν_{\parallel} and ν_{\perp} are the correlation length exponents. The results on the location of the critical wetting temperature [$T_w(h_1)$] and the critical exponents do not depend on this choice of c . The value was chosen simply because it generates small integers solutions for L and M : $(L, M) = (6, 32); (12, 128); (18, 288); (24, 512); (30, 800); (36, 1152); (48, 2048)$. The effect of considering other options of c is discussed in Ref. [13]. The panels in Fig. 2 show the temperature dependence of the first two moments of the magnetization $m = \sum_{i=1}^N s_i$, $\langle |m| \rangle$, $\langle m^2 \rangle$, as calculated using metropolis Monte Carlo simulations, for an applied field $h_1 = 0.7$. These are shown together with Binder's fourth-order cumulant U ,

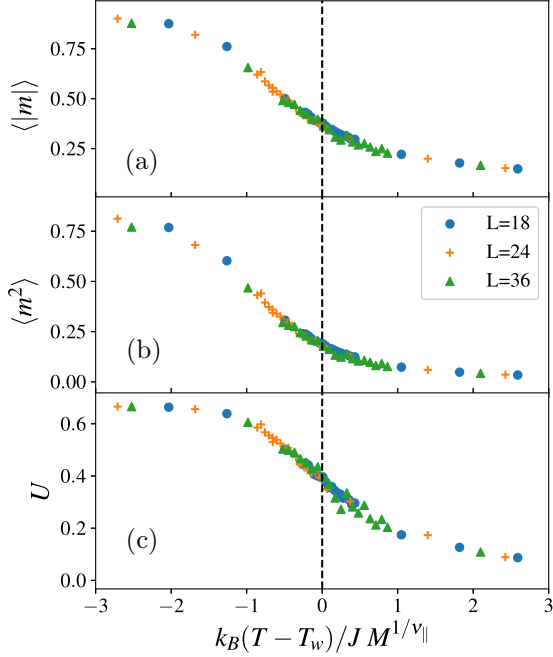


FIG. 3. Scaling plots for $\langle |m| \rangle$ (a), $\langle m^2 \rangle$ (b) and U (c), vs $k_B(T - T_w)/J M^{1/\nu_{\parallel}}$, where $\nu_{\parallel} = 2$. For the parameters $h_w = 0.7$, $\alpha = 1$, $D = 3$, and different values of L , as shown in the figure.

given by

$$U = 1 - \frac{\langle m^4 \rangle}{3\langle m^2 \rangle^2}. \quad (3)$$

As it can be seen in the figure, there is unique size-independent intersection point at a temperature $T = 1.30$. This behavior, not at all common in second-order phase transition, is a clear evidence of a transition that follows the type of scaling proposed by Albano and Binder [13], with a critical exponent for the order parameter given by $\beta = 0$. Note the full agreement between the size independent intersection points of all the measured quantities including the cumulant, where an intersection point is expected for a wetting transitions. This gives our first estimate of the wetting critical temperature for $h_1 = 0.7$, namely, $T_w(h_1) = 1.30$.

In the wet phase, the average position of the interface is in the middle of the lattice, between the rows $y = L/2$ and $y = L/2 + 1$, for L even; but due to capillary waves on the M scale in the x direction, the interface performs excursions of order \sqrt{M} in the y direction, which are of the order of $L/2$ for the choice of geometry proposed in Eq. (2).

In addition, Fig. 3 shows the collapse of the curves shown in Fig. 2 when $\langle |m| \rangle$, $\langle m^2 \rangle$ and U are plotted as a function of $k_B(T - T_w)/J M^{1/\nu_{\parallel}}$ with $\nu_{\parallel} = 2$, as proof of the scaling proposed by Albano and Binder. We observe a rather good data collapse, although there are deviations due to both statistical errors and systematic effects when M and/or χ are not large enough or when data is included too far from $T_w(h_1)$.

Figure 4 shows a scaling analysis of the heights and locations of the susceptibility peaks $k_B T/J \chi$, calculated using

$$k_B T/J \chi = LM(\langle m^2 \rangle - \langle |m| \rangle^2). \quad (4)$$

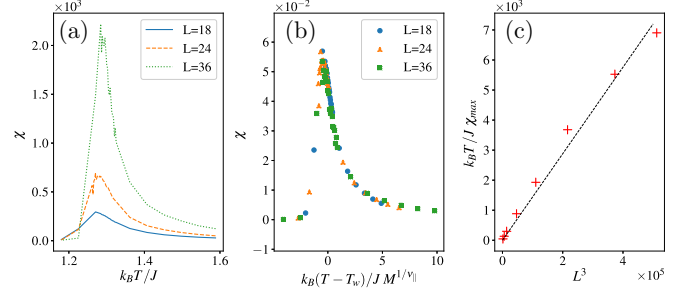


FIG. 4. Plot of susceptibility χ vs temperature $k_B T/J$ (a) for parameters $\alpha = 1$, $D = 3$, $h_1 = 0.7$. Collapse of the data of χ vs $k_B(T - T_w)/J M^{1/\nu_{\parallel}}$ (b). Finally, extrapolation of the peaks of χ to prove the power law scaling $k_B T/J \chi_{\max} \propto c^{1/2} M^{3/2 - 2\beta/\nu_{\parallel}} = M^{3/2} \propto L^3$, with $\beta = 0$ as in Ref. [13].

Figures 2, 3, and 4 are examples representative of the general pattern of behavior. Therefore, it can be concluded that by using the finite-size scaling analysis as presented here, wetting transitions for the Blume-Emery-Griffiths model can be located in a square lattice with reasonable accuracy.

Based on the results obtained for these scalings we have constructed the phase diagram of the wetting transition. Figure 5(a) shows the phase diagram in h_1 as a function of T_w/T_b , where T_b is the bulk transition temperature. Here one can see how as the surface field decreases, the wetting critical temperature tends to the value for a bulk transition. This effect is also present in the $D - k_B T/J$ phase diagram shown in Fig. 6.

In second-order phase transitions, h_1 obeys

$$h_1(T) \propto (T_b - T_w)^{\Delta_1}, \quad (5)$$

where Δ_1 is the critical exponent that controls the scaling behavior with the surface field h_1 near the criticality of the bulk. Abraham's exact solution ($\alpha = 0$) implies $\Delta_1 = 1/2$. Figure 5(b) shows h_1 vs $(T_b - T_w)^{1/2}$. Albeit with different prefactors, both cases follow the expected critical behavior.

These diagrams can be included in the phase diagram of the BEG model as shown in Fig. 6, for a better visualization of the results. Here one can see that, as it was mentioned before, when $h_1 \rightarrow 0$, the wetting transition moves towards the bulk

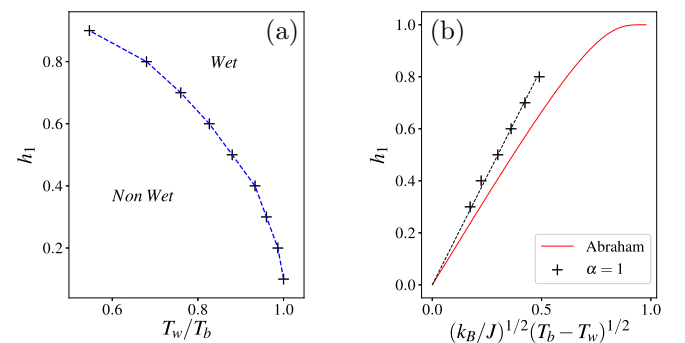


FIG. 5. (a) Plots of the wetting transitions h_1 vs T_w/T_b , with $T_b = 1.748$. The parameters used were $\alpha = 1$, $D = 3$. (b) Plots of the critical wetting surface fields h_1 vs $(k_B/J)^{\Delta_1}(T_b - T_w)^{\Delta_1}$, with $\Delta_1 = 1/2$, obtained for Abraham's exact solution ($\alpha = 0$) and the numerical data shown in the left-hand side panel.

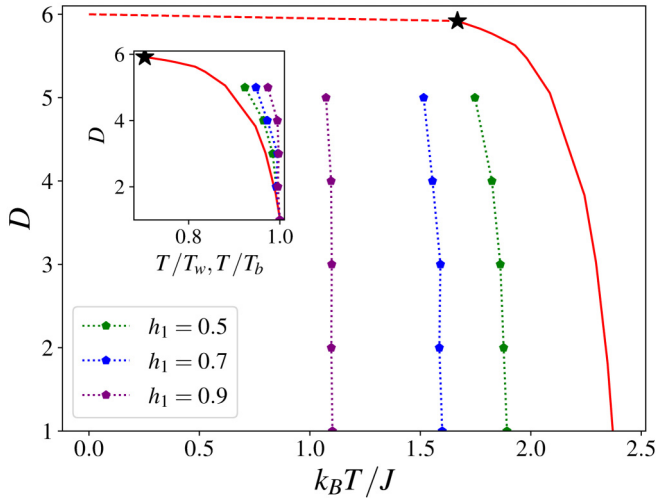


FIG. 6. Plots of the wetting transitions, this time in terms of D vs $k_B T/J$, for $\alpha = 2$ and different values of the surface field h_1 as shown in the figure. The red line represents the bulk phase diagram of the BEG model for $\alpha = 2$ in Ref. [42] in the absence of surface fields. Black star represents the tricritical point. In the inset the curves of the wetting transition and the bulk transitions are normalized by the wetting critical temperature and the bulk critical temperature, respectively.

transition. Moreover, it is easier to appreciate this behavior by normalizing the curves by the wetting critical temperature and the bulk critical temperature, respectively, as it is shown in the inset.

B. Interfacial adsorption

To characterize the interfacial adsorption one measures the excess of vacancies due to the interface, W_0 , defined as follows:

$$W_0 = L(f_0 - F_0), \quad (6)$$

where f_0 is the vacancy density when the system is under the effects of inhomogeneous surface fields ($h_1 = -h_L$), while F_0 corresponds to the case of homogeneous fields ($h_1 = h_L$), and has to be determined by means of additional MC simulations.

Figure 7 shows that, at T_w , W_0 presents an inflection point, so if the derivative is performed with respect to the temperature, the wetting transition will be characterized by a peak in dW_0/dT , while for sufficiently high temperatures, a negative peak will appear corresponding to the bulk transition. This behavior is also shown in Fig. 8 for $\alpha = 1$, $D = 3$ and different values of the surface field h_1 . On Fig. 8(a), one can see how the positive peaks shift toward higher temperatures as h_1 is decreased, in agreement with the wetting phase diagram shown in Fig. 5, while the peak corresponding to T_b remains at a fixed position regardless of the field. Finite-size effects can be seen in Fig. 8(b). The peaks become sharper as the system size is increased, and the variation of both transition temperatures, T_w and T_b , is very small for lattice sizes bigger than 24.

Figure 9 shows the derivative of the interfacial adsorption, dW_0/dT , as a function of the biquadratic interaction α . If D is kept constant and α increased, then one can observe, see

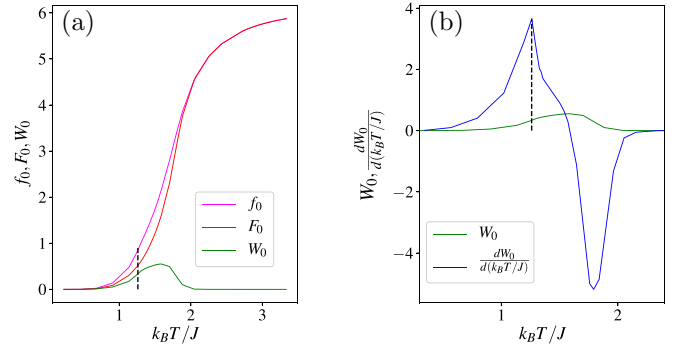


FIG. 7. Plots of the temperature dependence of the interfacial adsorption for a system with $\alpha = 1$, $D = 3$, $h_1 = 0.7$ and lattice size $L = 18$. (a) shows the vacancy densities for a system with and without an interface (f_0 and F_0 , respectively), as well as the difference between both (W_0). The enrichment of vacancies is clearly observed due to the interface near the critical wetting temperature $T_w = 1.30$ (black dashed line). (b) shows both W_0 and its derivative versus the temperature. It is observed that the maximum corresponds to the wetting transition, while the negative peak corresponds to the bulk transition for $T_b = 1.748$ as in Ref. [42].

Fig. 9(b), that while the interfacial adsorption decreases, the critical wetting temperature increases. This happens because the number of vacancies segregated at the interface increases as the system approaches the paramagnetic phase. In the case of $\alpha = 1$ the system is close to that phase, so the peak of the interfacial adsorption is greater than the one for $\alpha = 4$, which is very far from the paramagnetic phase. It is important to note that to help comparison between the different curves, both the $\alpha = 3$ curve and the $\alpha = 4$ curve were multiplied by a factor 10 and 100, respectively. However, as α increases, T_w increases since the attraction between the spins makes it more difficult for the interface to detach from the wall. This seems to indicate that the character of the transitions is not altered, even when the vacancies experiment a strong attractive interaction between them.

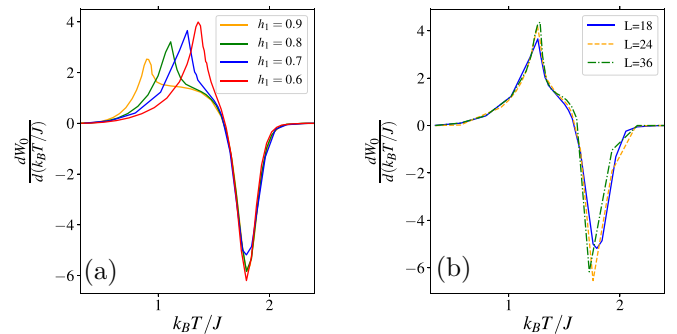


FIG. 8. Plots of the derivative of the interfacial adsorption of vacancies, $dW_0/d(k_B T/J)$ with respect to the temperature $k_B T/J$ for the parameters $\alpha = 1$, $D = 3$ and: different values of the surface field h_1 with lattice size $L = 18$ (a) and different lattice sizes (b). For these parameters, $T_w(h_1 = 0.7) = 1.30$ (maximum peak in the right-hand side panel) and $T_b = 1.748$ (minimum peak in both panels).

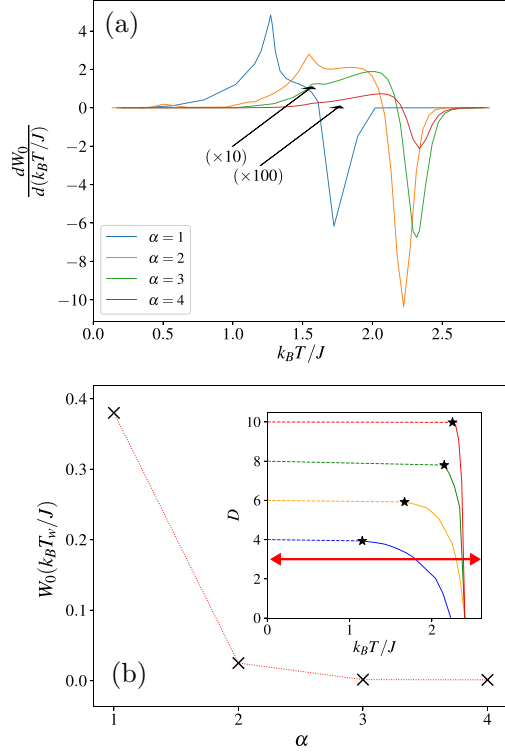


FIG. 9. Panel (a) shows the plots of the derivative of the interfacial adsorption of vacancies W_0 vs the temperature $k_B T/J$ for the parameters $D = 3$, $h_1 = 0.7$, lattice size $L = 36$ and different values of α . For reasons of scale, both the $\alpha = 3$ curve and the $\alpha = 4$ curve were multiplied by 10 and 100, respectively, to facilitate the comparison with $\alpha = 1$ and $\alpha = 2$ curves. Maximum peaks correspond to critical wetting transition while minimum peak correspond to bulk transition. The inset shows the region of interest, red arrow, as well as part of the four different phase diagrams [42] corresponding to each of the considered values of α . It can be seen that the study region moves away from the paramagnetic phase as α increases. Therefore, one observes that the interfacial adsorption decreases when approaching the bulk critical temperature for larger values of α (larger T_w). Panel (b) shows the interfacial adsorption at the wetting transition critical temperature $W_0(k_B T_w/J)$ vs α . Here one can see how the the interfacial adsorption of the vacancies on the interface decrease as α increase. It is because as α increase, the spins tend to stay together so a bigger value of D is needed to place the vacancies on the interface.

C. Finite-size scaling of the wetting interface

As previously mentioned, the interface between domains undergoes localization-delocalization transitions that depend on the temperature and the magnitude of the competitive surface fields. Those effective transitions are the precursors of the wetting transitions observed when the thermodynamic limit is properly taken. This localization-delocalization transition can be characterized by using the magnetization corresponding to those profiles [43] [Fig. 10(a)]. It is important to point out that while in the wet state the interface is unbound from either wall and fluctuates around the midpoint position, for partial wetting the interface could be bound to layers $n = 1$ or $n = L$, with equal probability. For simplicity, Fig. 10(a) only shows the case in which the interface is attached to layer $n = 1$. By

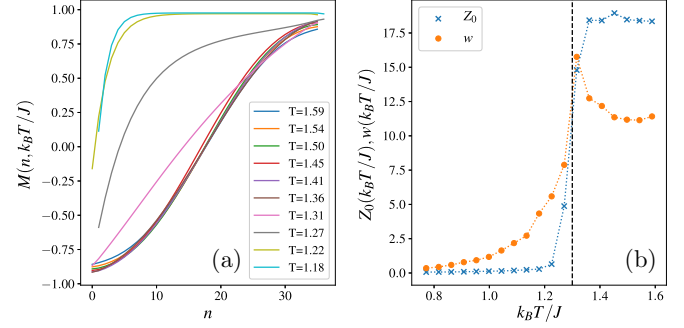


FIG. 10. (a) Plot of the magnetization profiles $M(n, k_B T/J)$ for $\alpha = 1$, $D = 3$, $h_1 = 0.7$, lattice size $L = 36$ and different values of temperature. (b) Plot of the interface average location $Z_0(k_B T/J)$ and the interface effective width $w(k_B T/J)$ vs the temperature, obtained from the magnetization profiles. The black dashed line represents the wetting critical temperature $T_w = 1.30$ just for reference.

fitting the numerical curves with the aid of an error function $M(n, T) = -m_0 \text{erf}[(n - Z_0)/2w(T)]$, where n is the layer number and m_0 is of the order of the bulk spontaneous magnetization which is obtained for $n > L/2$, one can evaluate both the *effective* width of the interface $w(T)$ [not to be confused with the interfacial adsorption $W(T)$] as well as its average location $Z_0(T)$. In Fig. 10(b) we can observe how Z_0 evolves from being attached to one of the walls to finally fluctuate around the middle of the system after reaching the critical wetting temperature.

By taking advantage of the interfacial adsorption of the vacancies we can also obtain $Z_0^v(T)$ and $w^v(T)$, where the superindex v refers to vacancies, by following a similar method used to compute the interfacial adsorption W . Instead of subtracting the vacancy density both when the system is under the effects of inhomogeneous and homogeneous fields as it was previously done, we subtract the respective vacancy profiles. This gives us the vacancy excess profile $V(n, T)$ [Fig. 11(a)], which can be fitted by a Gaussian function given by $V(n, T) = v_0 \exp\{-[n - Z_0^v(T)]^2/[2w^v(T)^2]\}$ to find $Z_0^v(T)$ and $w^v(T)$, as shown in Fig. 11(b). Notice that, as in the already

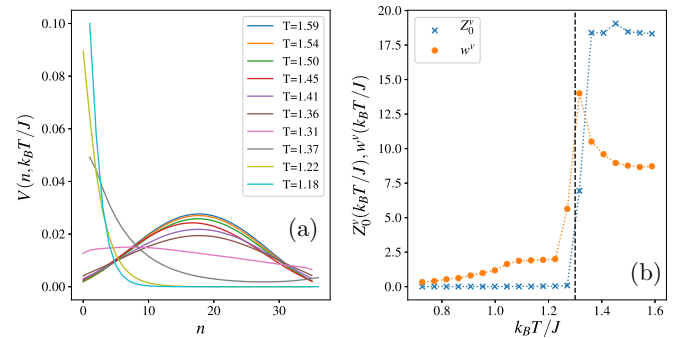


FIG. 11. (a) Plot of the vacancy excess profiles $V(n, k_B T/J)$ for $\alpha = 1$, $D = 3$, $h_1 = 0.7$, lattice size $L = 36$ and different values of temperature. (b) Plot of the interface average location $Z_0^v(k_B T/J)$ and the interface effective width $w^v(k_B T/J)$ vs the temperature, obtained from the vacancy excess. The black dashed line represents the wetting critical temperature $T_w = 1.30$ just for reference.

commented case of Fig. 10(a), Fig. 11(a) corresponds to profiles taken with the interface attached to the wall at $n = 1$.

Let us now recall that Z_0 can be expressed in terms of a dynamic scaling ansatz [44,45] similar to the scaling approach used in domain growth [46], yielding

$$Z_0(t, \xi_{\parallel}) = b^{-\beta_s} Z_0^{(1)}(b^{-\nu_{\parallel} z} t, b \xi_{\parallel}^{-1/\nu_{\parallel}}), \quad (7)$$

where t is the time, b is a scale factor, ξ_{\parallel} is the correlation length for interfacial fluctuations in the direction parallel to the wall, ν_{\parallel} is the corresponding correlation length exponent, z is a dynamic exponent, and β_s is the static exponent describing the divergence of the distance of the interface from the wall. $Z^{(1)}$ denotes a scaling function (as well as $Z^{(2)}$, $Z^{(3)}$, and $Z^{(4)}$ below). For the case of critical wetting, i.e. in the absence of bulk field and close to the wetting critical point we define $\tau = |T - T_w|$, so that $\xi_{\parallel} \simeq \tau^{-\nu_{\parallel}}$. Then Eq. (7) becomes

$$Z_0(t, \tau) = b^{-\beta_s} Z_0^{(2)}(b^{-\nu_{\parallel} z} t, b \tau). \quad (8)$$

Noting that static scaling at wetting transitions in $d = 2$ implies $Z_0(t \rightarrow \infty) \propto \xi_{\perp} \propto \xi_{\parallel}^{\zeta}$ with the ‘‘wandering exponent’’ $\zeta = 1/2$, one generally concludes in $d = 2$ that $\nu_{\perp} = \beta_s = \nu_{\parallel}/2$. Additionally, $Z_0 \propto \xi_{\perp}$ implies that the profile perpendicular to the surface is characterized by a single length scale.

Now, by taking $t \rightarrow \infty$ and $b = L^a$ with arbitrary a we obtain

$$Z_0(\tau, L) = L^{-a\beta_s} Z_0^{(3)}(L^a \tau). \quad (9)$$

To get $a\beta_s = 1$, a must be $-1/\beta_s = 1/\nu_{\perp}$ then

$$Z_0(\tau, L) = L Z_0^{(4)}\left(L^{\frac{1}{\nu_{\perp}}} \tau\right). \quad (10)$$

However, since [43] $Z_0 \sim \tau^{\beta_s} \sim \tau^{-\nu_{\perp}}$ and $Z_0 \sim L(L^{1/\nu_{\perp}} \tau)^x$, by taking $x = -\nu_{\perp} = -1$ we get

$$Z_0 \propto |T - T_w|^{-1}. \quad (11)$$

Similar scaling behavior can be obtained for $w(\tau, L)$, namely, $w(\tau, L) = L w(L^{1/\nu_{\parallel}} \tau)$ which can be derived just by assuming $w(k_B T/J) \propto |T - T_w|^{-\nu_{\parallel}}$.

Figure 12 shows that Eq. (11) holds for $Z_0(k_B T/J)$ and $w(k_B T/J)$ both for magnetization profiles and vacancies excess profiles [note that the quantities referred to the vacancy excess are labeled by the superindex v , i.e., $Z_0^v(T)$ and $w^v(T)$]. This is shown for $\alpha = 1$, $D = 3$, $h_1 = 0.7$ and different lattice sizes, but also for $\alpha = 2$, $D = 3$, $h_1 = 0.7$, and $\alpha = 2$, $D = 5$, $h_1 = 0.7$ in Fig. 13.

D. Thermodynamic integration

Another method frequently used to characterize wetting transitions, particularly those of the first order, is the Thermodynamic Integration. This method allows to determine the location of the coexistence points in the phase diagram or, in other words, find the field values for each temperature in which the phase transitions occur. It has been previously used successfully to locate wetting transitions in $d = 3$ in Ref. [47] and $d = 2$ in Refs. [13,19]. For a more detailed description and discussion of this method, refer to Refs. [48,49].

To locate wetting transitions, we consider the fact that they depend on the difference in excess surface free

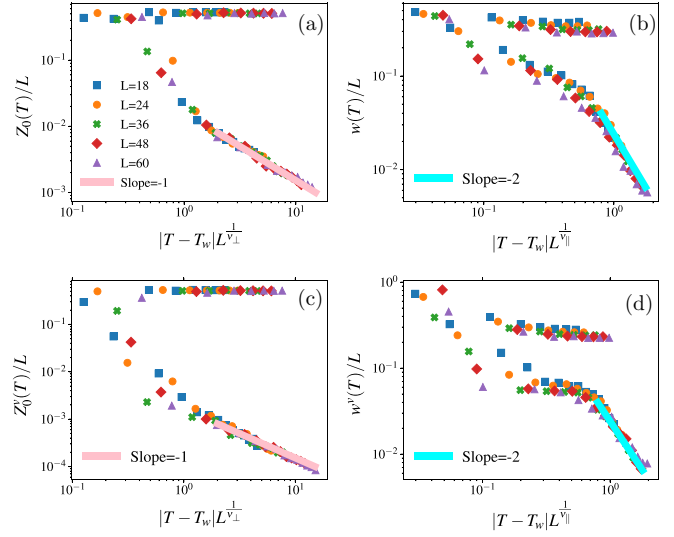


FIG. 12. Log-log plots of the $Z_0(k_B T/J)$ [panels (a) and (c)] and $w(k_B T/J)$ [panels (b) and (d)] scaling for $\alpha = 1$, $D = 3$, $h_1 = 0$ and different lattice size. Upper panels were made by using magnetization profiles while lower panels were made by using vacancy excess profiles. In both cases Eq. (11) holds. Solid lines represent the linear fitting with slopes = -1 and = -2 , respectively, and they have been drawn to guide the eyes.

energy ($\Delta f_{1L} = f_s^+ - f_s^-$) between semi-infinite domains with positive (+) and negative (-) magnetization. Signs of magnetization are caused by surface fields and interfacial tension between the coexisting phases $f_{\text{int}}(T)$. This, according to Young’s [4] criterion, satisfies $f_s^+ - f_s^- = f_{\text{int}}$. For the Ising

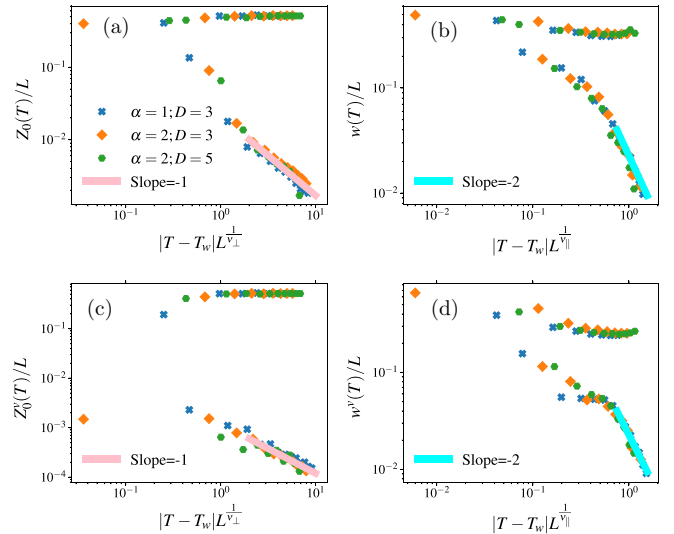


FIG. 13. Log-log plots of the $Z_0(k_B T/J)$ [panels (a) and (c)] and $w(k_B T/J)$ [panels (b) and (d)] scaling as obtained for a lattice of side $L = 36$ and different values of α and D versus $k_B |T - T_w|/J L^{\frac{1}{\nu_{\perp}}}$. Upper panels were made by using magnetization profiles while lower panels were made by using vacancy excess profiles. In both cases Eq. (11) holds. Solid lines represent the linear fitting with slopes = -1 and = -2 , respectively, and they have been drawn to guide the eyes.

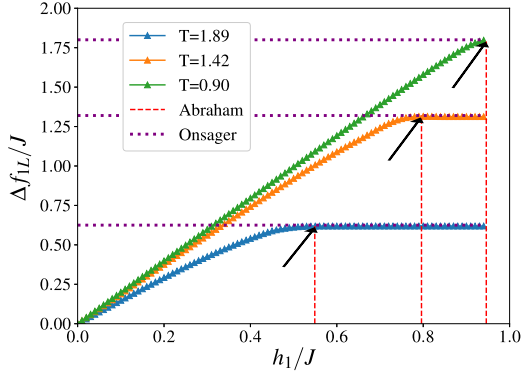


FIG. 14. Plot of $\Delta f_{1L}/J$ in function of the surface field h_1/J , obtained for different temperatures, with $\alpha = 0$ and $D = -\infty$, that is, Ising model. The horizontal lines correspond to the interfacial free energy, which is obtained from Onsager's exact solution [50], while the vertical lines correspond to the critical fields for which wetting transitions occur, and are obtained from Abraham's exact solution [47]. The intersection points are indicated by arrows.

model, the interfacial free energy is known exactly thanks to the Onsager [50] solution,

$$\sigma = 2J + k_B T \log \left[\tanh \left(\frac{J}{k_B T} \right) \right]. \quad (12)$$

But in this work it is necessary to use the thermodynamic integration. First, we use the following relations:

$$m_1 = - \left(\frac{\partial f_s(T, h_1)}{\partial h_1} \right)_T, \quad (13)$$

$$m_L = - \left(\frac{\partial f_s(T, h_L)}{\partial h_L} \right)_T, \quad (14)$$

which connect the surface magnetization on the walls 1 and L , with the surface free energy and the corresponding surface field. In this way, the difference of surface free energy excess (Δf_{1L}) can be obtained as follows:

$$\begin{aligned} \Delta f_{1L} &= f_s(T, h_1) - f_s(T, h_L), \\ &= \int_0^{h_1} (m_L - m_1) dh'_1. \end{aligned} \quad (15)$$

To evaluate this integral, we took $h_L = -h_1$. The system size was $L = 36$ and $M = 1152$, and its initial configuration consisted of all spins pointing up. In addition, averages of more than 10×10^6 MCS were taken, after discarding the first 2×10^6 MCS. As proof of the accuracy of this procedure, the case $D = -\infty$ was first studied, in which vacancies are excluded and the standard wetting problem is obtained in the Ising model $d = 2$, for which the exact solution is known thanks to Abraham [47].

Figure 14 shows the results for Δf_{1L} in terms of h_1 obtained for $D = -\infty$. It was found that the Eq. (15) can be discretized in steps of $h_1 = 0.025$ so that the numerical integration error is small enough (note that the fields are also indicated in units of J). Since in the case of the Ising model the interfacial free energy is known exactly according to Onsager Eq. (12), in Fig. 14 the values used for σ corresponding to the temperature used to perform the integration of Eq. (15) were

included (horizontal lines). In addition, Abraham's exact results were included for the critical fields of wetting transitions (vertical lines), which intercept the integration curves just when they begin to saturate and coincide (within statistical error) with the lines that define the interfacial free energy. Therefore, Fig. 14 shows that by using thermodynamic integration and taking advantage of the existence of exact results, the location of wetting transitions is compatible with the exact results.

Unfortunately, in the case of $D > -\infty$, there is no exact solution of σ , so interfacial free energy must also be evaluated through thermodynamic integration.

For this purpose, two system reference states are used: one with all the spins pointing up (+1), and one in which half the spins are pointing up and the other half is pointing down. In this way, by using the relationship between free energy and internal energy by spin [48,49]

$$u = \left(\frac{\partial(\beta f)}{\partial \beta} \right)_{\alpha, D, h_1, h_L}, \quad (16)$$

where $\beta = 1/T$, one can perform the following integration

$$\beta f(\beta) = \beta_0 f(\beta_0) + \int_{\beta_0}^{\beta} u(\beta') d\beta'. \quad (17)$$

Here β_0 represents a reference state and β the state at the working temperature, that is, the temperature at which the transition is intended to be found. The most tempting option is to take $\beta_0 = 0$, but, since we are going to analyze temperatures below the critical temperature of the system, this is not convenient. An alternative is to consider $T = 0$ as a reference state, where the entropy is zero and the free energy can be considered equal to internal energy by virtue of the relationship

$$U = F + TS. \quad (18)$$

In numerical implementation, it will be enough to take a temperature that is not zero but too small to consider entropic contributions irrelevant. For example, $T = 0.05$, that is $\beta_0 = 20$, is small enough to omit such contributions.

This procedure is simplified when using the Wang-Landau algorithm, which allows you to directly calculate the free energy of the system. To do this, the partition function of the two reference states are calculated: one with all the spins pointing up and the other with one half pointing up and the other down. To obtain the interface in the latter case, antiperiodic boundary conditions were imposed. Then, the free energy for both cases are calculated and subtracted as follows:

$$f_{\text{interfacial}} = f^{\pm} - f^+, \quad (19)$$

where f^{\pm} is the free energy of the system with interface and f^+ is the free energy of the system without interface. Since the energy excess f^{\pm} is caused by the interface, $f_{\text{interfacial}}$ is the interfacial free energy. In this way it is possible to calculate the energy for any value of α and D .

Figures 15(a) and 15(b) show the plots of σ as a function of T/T_b obtained for $\alpha = 0$ and $\alpha = 1$, respectively, and different values of D . For $D = -\infty$, the error bars of the numerical integration are smaller than the line size. However, for finite values of D , the interfacial free energy decreases (at constant

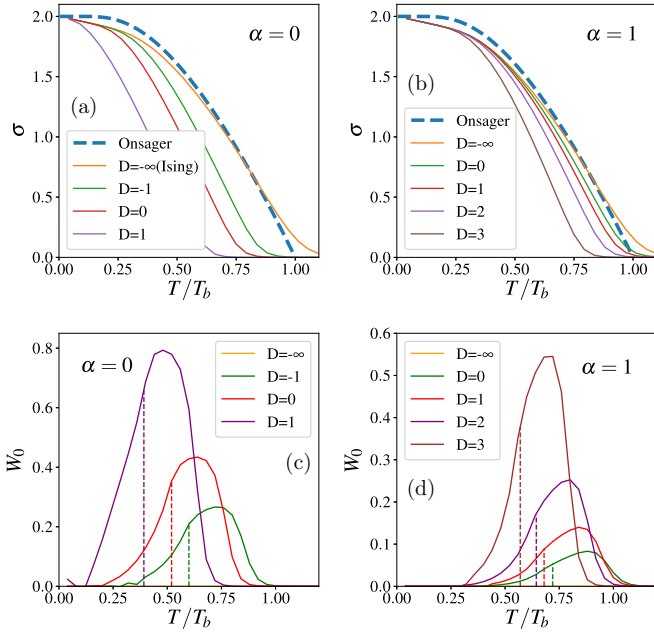


FIG. 15. Panels (a) and (b) show the interfacial free energy σ in terms of T/T_b , for $\alpha = 0$ and $\alpha = 1$, respectively, with different values of D . The results obtained for the Ising model ($D = -\infty$ and $\alpha = 0$) show a slight departure from Onsager's exact solution (dotted line), due to finite-size effects ($L = 16$ in the simulation). Panels (c) and (d) show the interfacial adsorption in terms of T/T_b , for $\alpha = 0$ and $\alpha = 1$, respectively. Dashed lines represent wetting critical temperatures and they have been drawn to guide the eyes.

temperature) compared to the case of Ising due to the presence of non-magnetic impurities in the interface, as expected. That increment of the vacancies in the interface can be seen in the lower panels, *c* and *d*, in which the interfacial adsorption W_0 increases as D increase. However, Fig. 16, shows how the interfacial free energy increases when α increase for a constant value of D . This is caused by the decrease in the amount of vacancies in the interface as the system moves away

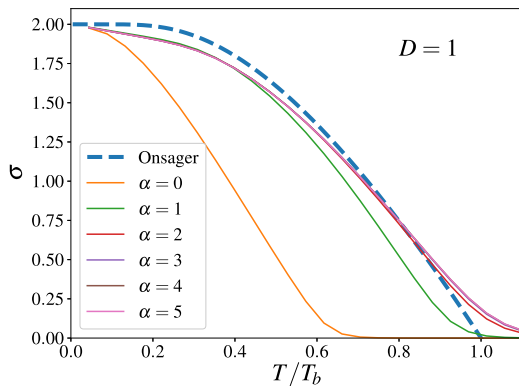


FIG. 16. Plot of the interfacial free energy σ in terms of T/T_b , for $D = 1$, with different values of α . The results obtained for the Ising model ($D = -\infty$ and $\alpha = 0$) show a slight shift with respect to the exact Onsager solution (dotted line), due to the size of the lattice ($L = 16$).

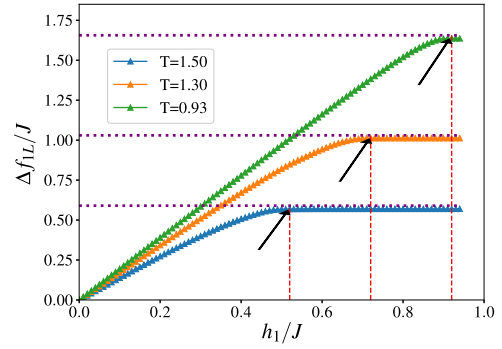


FIG. 17. Plots of $\Delta f_{1L}/J$ in terms of the surface field h_1/J obtained for different temperatures, with $\alpha = 1$ and $D = 3$. Horizontal lines correspond to the interfacial free energy obtained by thermodynamic integration (see Fig. 15). The intersection points for the second-order wetting transitions are indicated by arrows. It is important to note that these points are in agreement with those shown in Sec. III A.

from the paramagnetic phase. It is in complete agreement with Fig. 9.

Finally, Fig. 17 shows the plots of the integration results of Δf_{1L} in terms of h_1 , obtained for $D = 3$, $\alpha = 1$ and different temperature values. As in Fig. 14, the values of σ obtained by thermodynamic integration were included, and the values of the critical fields, obtained from the plots of Fig. 5. The results are in agreement with those shown in Figs. 3, 4, and 8 for $h = 0.7$.

This method is also very useful when working with first-order transitions, where one cannot perform finite-size scaling.

IV. CONCLUSIONS

We studied the wetting behavior of the two-dimensional Blume-Emery-Griffiths model confined in a strip with competing boundary fields by means of Monte Carlo simulations. The BEG model has a biquadratic interaction term which allows us to control the interaction between vacancies by tuning the biquadratic constant α . We proved that a previously proposed anisotropic scaling proposed by Albano and Binder is still valid for the BEG model. We assumed that if the vacancies tend to cluster in the interface, its behavior would be analogous to the one of the interfacial pinning induced by impurities so the character of the transition would change, as have been shown by Albano and Binder [13]. But our study on both the influence of the biquadratic interaction and the role of interfacial adsorption on wetting transitions reveals that regardless of how intense the attraction between vacancies is, the nature of the transition does not change from second to first order.

Wetting transition lines have been determined for different values of h_1 , D , and α . To estimate T_w , the calculation of the second moment of the magnetization and the Binder cumulant proved very useful, showing only weak effects of finite size. It was shown that as h_1 increases, T_w decreases, while when $h_1 \rightarrow 0$, $T_w \rightarrow T_b$. However, the presence of non-magnetic impurities (vacancies) can favor the wetting transition

depending on D and α . Finally, the thermodynamic integration method was used to verify second-order transitions. This method is very useful when working with first-order transitions, in which it is not possible to perform a finite-size scaling; however, all the transitions were second order.

The adsorption of vacancies at the interface between regions rich with spins -1 and 1 was also studied. Adsorption was shown to grow rapidly near T_w , possibly associated with a singularity in the derivative of W_0 with respect to temperature. However, if D is kept constant and α is increased, then the system will need a higher temperature to reach the wetting transition. This method allows us to locate wetting and bulk transitions precisely and easily.

We showed that due to the interfacial adsorption of the vacancies, wetting transitions can also be characterized by means of the vacancy excess profiles. As we approach the wetting critical temperature the interface detached from the wall and start to fluctuate in the middle of the layer. So, if we measure the average position of the interface, when reaching the wetting critical temperature, then it will be fluctuating around $L/2$. It holds for different values of D and α .

These features reported in the present paper could be relevant for practical applications aimed at designing highly stable superhydrophobic and omniphobic materials.

APPENDIX: NUMERICAL METHODS

The metropolis update (MU) is a Markov chain Monte Carlo method that allows to obtain a sequence of random samples from a probability distribution. Simulations are started from a random configuration of spins and vacancies. Then the energy E_i of this initial configuration is computed, and subsequently a new configuration, with energy E_j , is attempted just by flipping a randomly selected spin (or vacancy). The transition probability between those configurations, given by $\omega = \exp[\beta(E_j - E_i)]$; $\beta = 1/k_B T$ is evaluated, and the trial is accepted if $\omega > r$, where $r \in (0, 1)$ is a pseudo random number and $k_B T$ is the Boltzmann constant. A Monte Carlo time step (MCS) involves $N = L \times M$ flipping attempts, so that each spin of the system is visited once in average. This procedure is followed during $\tau_D = 2 \times 10^6$ MCS to allow for the equilibration of the system. Then, data is recorded during $\tau_M = 10 \times 10^6$ MCS, to perform an average over the quantities of interest, such as magnetization, susceptibility, cumulant, etc.

Even though this is a very useful algorithm to study many particles systems, in the case of the BEG model it shows some disadvantages that are successfully solved by the Wang-Landau algorithm. Among others, we can quote that the MU algorithm works properly if all the configurations of the system are into a relatively narrow energy range, otherwise, there is the possibility that, during the random walk, the process gets stuck in an energy local minimum from where, the probability to escape is very low. Furthermore, the MU method only allows to set one temperature per run, so one has to perform many runs to get the data for many temperatures.

Unlike the usual MU algorithm that directly estimates the mean values of the thermodynamic observables at a given temperature, the Wang-Landau (WL) algorithm accurately estimates the density of states g via a random walk. We work

in the grand canonical ensemble, interpreting D in the second term of the BEG Hamiltonian to be a chemical potential. The number of spins/particles is then given by $\mathcal{N} = \sum_{i=1}^N s_i^2$. The energy E is given solely by the interaction terms: the first, third, fourth and fifth terms of Eq. (1). To compute the grand-canonical partition function and calculate the thermodynamic quantities under an applied magnetic field we seek to determine $g(E, \mathcal{N}, m)$, where $m = \sum_{i=1}^N s_i$ is the magnetization. The algorithm samples the configuration space by randomly flipping spins. New configurations of the system are accepted with a probability that is proportional to $1/g(E, \mathcal{N}, m)$, the reciprocal of the density of states. As a result a flat histogram $HE(E, \mathcal{N}, m)$ is generated during the random walk and the current density of states is modified by a refinement parameter f . Since the density of states is not known *a priori*, in the beginning of the simulation one sets all entries to $g(E, \mathcal{N}, m) = 1$ for every state and perform a random walk considering that, if $(E_1, \mathcal{N}_1, m_1)$ and $(E_2, \mathcal{N}_2, m_2)$ are the states before and after a spin is flipped, the transition probability would be

$$p[(E_1, \mathcal{N}_1, m_1) \rightarrow (E_2, \mathcal{N}_2, m_2)] = \min\left(\frac{g(E_1, \mathcal{N}_1, m_1)}{g(E_2, \mathcal{N}_2, m_2)}, 1\right), \quad (\text{A1})$$

and the density of states is modified as

$$g(E, \mathcal{N}, m) \rightarrow g(E, \mathcal{N}, m)f. \quad (\text{A2})$$

When choosing the refinement parameter, one should have in mind that all possible energy levels must be reached quickly even for a large system. A reasonable choice is $f = f_0 = e$, and to reduce it one can use a function like $f_{n+1} = \sqrt{f_n}$. This reduction is accomplished whenever the histogram becomes flat during the random walk. In our simulations, the flatness criterion for the histogram is about 80% of the average histogram $\langle HE(E, \mathcal{N}, m) \rangle$ and is generally checked every 1000 MC steps. Afterwards, the histogram is reset to 0 and the simulation comes to an end when the modification factor is smaller than $1e^{-8}$. Convergence of large systems is always difficult in the WL algorithm, moreover, every time a new parameter is added to g the convergence becomes much harder since it requires smoothness on a higher dimensional space. In our case we require smoothness on a three-dimensional space, which limited the size of our simulations. We have used the modification proposed by Belardinelli and Pereyra (BP), which changes the refinement parameter to $1/\tau$, where $\tau = j/\epsilon$ is the Monte Carlo time, j is the number of trial moves attempted and ϵ is the number of energy levels of the system. Starting from the same initial condition as the original WL algorithm, the modification factor is reduced as $1/\tau$, instead of checking the flatness condition after the condition $f_n \leq 1/t$. The final value of f should be fixed from the beginning. One additional advantage of the BP implementation is that its faster convergence speed makes it unnecessary to partition the energy spectrum. Thus, the full energy range can be used in all simulations and artifacts close to first-order transitions characteristic to multirange implementations are avoided.

We have estimated the error of our simulations by looking at the different particular cases where our model has an exact solution. In all cases the error of the simulated data is smaller than the symbol size of the figures.

- [1] A.-L. Barabási and H. E. Stanley, *Fractal Concepts in Surface Growth* (Cambridge University Press, Cambridge, UK, 1995).
- [2] J. Kertész and T. Vicsek, Self-affine interfaces, in *Fractals in Science*, edited by A. Bunde and S. Havlin (Springer, Berlin, 1994), pp. 89–118.
- [3] D. E. Sullivan and M. M. T. da Gama, Wetting transitions and multilayer adsorption at fluid interfaces, in *Fluid Interfacial Phenomena*, edited by C. Croxton (Wiley, New York, 1986), pp. 45–134.
- [4] S. Dietrich, *Physica A* **168**, 160 (1990).
- [5] M. Schick, Liquids at Interfaces, in *Proceedings of the Les Houches Summer School Lectures*, edited by J. Charvolin, J.-F. Joanny, and J. Zinn-Justin (Elsevier, Amsterdam, 1990), p. 415.
- [6] G. Forgacs, R. Lipowsky, and T. M. Nieuwenhuizen, The behavior of interfaces in ordered and disordered systems, in *Phase Transitions and Critical Phenomena*, edited by C. Domb and J. Lebowitz, Vol. 14 (Academic Press, San Diego, CA, 1991), pp. 135–364.
- [7] D. Bonn and D. Ross, *Rep. Prog. Phys.* **64**, 1085 (2001).
- [8] P. G. de Gennes, F. Brochard-Wyart, and D. Quere, *Capillarity and Wetting Phenomena: Drops, Bubbles, Pearls, Waves* (Springer-Verlag, New York, 2003).
- [9] T. Kissinger, A. Kotowicz, O. Kurz, F. Ginelli, and H. Hinrichsen, *J. Stat. Mech.: Theory Exp.* (2005) P06002.
- [10] J. Candia and E. V. Albano, *Phys. Rev. Lett.* **88**, 016103 (2001).
- [11] M. R. Moldover and J. W. Cahn, *Science* **207**, 1073 (1980).
- [12] W. Selke, *Surf. Sci.* **144**, 176 (1984).
- [13] E. V. Albano and K. Binder, *Phys. Rev. E* **85**, 061601 (2012).
- [14] N. Fytas and W. Selke, *Eur. Phys. J. B* **86**, 365 (2013).
- [15] E. V. Albano and K. Binder, *Phys. Rev. Lett.* **109**, 036101 (2012).
- [16] A. Pérez-Junquera, V. I. Marconi, A. B. Kolton, L. M. Álvarez-Prado, Y. Souche, A. Alija, M. Vélez, J. V. Anguita, J. M. Alameda, J. I. Martín, and J. M. R. Parrondo, *Phys. Rev. Lett.* **100**, 037203 (2008).
- [17] V. I. Marconi, A. B. Kolton, J. A. Capitán, J. A. Cuesta, A. Pérez-Junquera, M. Vélez, J. I. Martín, and J. M. R. Parrondo, *Phys. Rev. B* **83**, 214403 (2011).
- [18] S. M. Cotes and E. V. Albano, *Phys. Rev. E* **83**, 061105 (2011).
- [19] M. L. Trobo, E. V. Albano, and K. Binder, *Phys. Rev. E* **90**, 022406 (2014).
- [20] M. Blume, V. J. Emery, and R. B. Griffiths, *Phys. Rev. A* **4**, 1071 (1971).
- [21] M. Blume, *Phys. Rev.* **141**, 517 (1966).
- [22] H. Capel, *Physica* **32**, 966 (1966).
- [23] A. Benyoussef, H. Ez-Zahraouy, H. Mahboub, and M. Ouazzani, *Physica A* **326**, 220 (2003).
- [24] R. Miranda, E. V. Albano, S. Daiser, G. Ertl, and K. Wandelt, *Phys. Rev. Lett.* **51**, 782 (1983).
- [25] R. Miranda, E. V. Albano, S. Daiser, K. Wandelt, and G. Ertl, *J. Chem. Phys.* **80**, 2931 (1984).
- [26] K. Binder, D. Landau, and M. Müller, *J. Stat. Phys.* **110**, 1411 (2003).
- [27] E. Albano, K. Binder, D. W. Heermann, and W. Paul, *Surf. Sci.* **223**, 151 (1989).
- [28] E. Albano, K. Binder, D. W. Heermann, and W. Paul, *J. Stat. Phys.* **61**, 161 (1990).
- [29] A. O. Parry and R. Evans, *Phys. Rev. Lett.* **64**, 439 (1990).
- [30] A. O. Parry and R. Evans, *Physica A* **181**, 250 (1992).
- [31] K. Binder, D. P. Landau, and A. M. Ferrenberg, *Phys. Rev. Lett.* **74**, 298 (1995).
- [32] K. Binder, D. P. Landau, and A. M. Ferrenberg, *Phys. Rev. E* **51**, 2823 (1995).
- [33] K. Binder, R. Evans, D. P. Landau, and A. M. Ferrenberg, *Phys. Rev. E* **53**, 5023 (1996).
- [34] E. Albano, K. Binder, and W. Paul, *J. Phys.: Condens. Matter* **12**, 2701 (2000).
- [35] B. J. Schulz, K. Binder, and M. Müller, *Phys. Rev. E* **71**, 046705 (2005).
- [36] K. Binder and D. P. Landau, *Phys. Rev. B* **37**, 1745 (1988).
- [37] K. Binder, D. P. Landau, and S. Wansleben, *Phys. Rev. B* **40**, 6971 (1989).
- [38] N. Metropolis, A. W. Rosenbluth, M. N. Rosenbluth, A. H. Teller, and E. Teller, *J. Chem. Phys.* **21**, 1087 (1953).
- [39] F. Wang and D. P. Landau, *Phys. Rev. Lett.* **86**, 2050 (2001).
- [40] F. Wang and D. P. Landau, *Phys. Rev. E* **64**, 056101 (2001).
- [41] R. E. Belardinelli and V. D. Pereyra, *Phys. Rev. E* **75**, 046701 (2007).
- [42] L. M. Luque, S. A. Grigera, and E. V. Albano, *J. Stat. Mech.: Theory Exp.* (2019) 033210.
- [43] E. V. Albano, A. De Virgiliis, M. Müller, and K. Binder, *J. Phys.: Condens. Matter* **18**, 2761 (2006).
- [44] R. Lipowsky, *J. Phys. A: Math. Gen.* **18**, L585 (1985).
- [45] K. Binder, in *Growth Kinetics of Wetting Layers at Surfaces*, edited by M. G. Lagally, Kinetics of Ordering and Growth at Surfaces, Vol. 239 (Springer US, New York, NY, 1990).
- [46] A. Sadiq and K. Binder, *J. Stat. Phys.* **35**, 517 (1984).
- [47] D. B. Abraham, *Phys. Rev. Lett.* **44**, 1165 (1980).
- [48] D. P. Landau and K. Binder, *A Guide to Monte Carlo Simulations in Statistical Physics*, 3rd ed. (Cambridge University Press, Cambridge, UK, 2009).
- [49] K. Binder, *Z. Phys. B* **45**, 61 (1981).
- [50] L. Onsager, *Phys. Rev.* **65**, 117 (1944).